EXHIBIT H

Linking Ligand-Induced Alterations in Androgen Receptor Structure to Differential Gene Expression: A First Step in the Rational Design of Selective Androgen Receptor Modulators

Dmitri Kazmin, Tatiana Prytkova, C. Edgar Cook, Russell Wolfinger, Tzu-Ming Chu, David Beratan, J. D. Norris, Ching-yi Chang, and Donald P. McDonnell

Department of Pharmacology and Cancer Biology (D.K., J.D.N., C.-y.C., D.P.M.), Duke University Medical Center, and Department of Chemistry (T.P., D.B.), Duke University, Durham, North Carolina 27710; Science and Engineering Group (C.E.C.), Research Triangle Institute, Research Triangle Park, North Carolina 27709; and SAS Institute (R.W., T.-M.C.), Cary, North Carolina 27513

We have previously identified a family of novel androgen receptor (AR) ligands that, upon binding, enable AR to adopt structures distinct from that observed in the presence of canonical agonists. In this report, we describe the use of these compounds to establish a relationship between AR structure and biological activity with a view to defining a rational approach with which to identify useful selective AR modulators. To this end, we used combinatorial peptide phage display coupled with molecular dynamic structure analysis to identify the surfaces on AR that are exposed specifically in the presence of selected AR ligands. Subsequently, we used a DNA microarray analysis to demonstrate that differently conformed receptors facilitate distinct patterns of gene expression in LNCaP cells. Interestingly, we observed a complete overlap in the identity of genes expressed after treatment with mechanistically distinct AR ligands. However, it was differences in the kinetics of gene regulation that distinguished these compounds. Follow-up studies, in cell-based assays of AR action, confirmed the importance of these alterations in gene expression. Together, these studies demonstrate an important link between AR structure, gene expression, and biological outcome. This relationship provides a firm underpinning for mechanism-based screens aimed at identifying SARMs with useful clinical profiles. (*Molecular Endocrinology* 20: 1201–1217, 2006)

STEROID HORMONE receptors are ligand-dependent transcription factors involved in the regulation of a wide range of physiological processes ranging from reproduction to cellular metabolism and homeostasis. In addition, inappropriate production of steroids or a change in the way the steroid-receptor (SR) complex is recognized by target cells underlies the pathology of many diseases. Not surprisingly, therefore, agents that positively or negatively regulate the action of this class of receptors have found widespread clinical use in the treatment of a diverse range of endocrinopathies. For the most part, the need for agonists and antagonists for each member of this

receptor family has been satisfied by the currently available compounds/drugs. Consequently, attention has shifted toward the exploitation of our current understanding of SR action to develop compounds, whose actions at their cognate receptors allow their activities to be manifest in a tissue- and process-selective manner.

In general terms, the cellular response to a given steroid hormone can be considered a composite of both its genomic and nongenomic activities. The latter describes the rapid responses to steroid-occupied receptors observed *in vitro* that result in the activation or modulation of cell signaling pathways (*i.e.* MAPK) (1, 2). The mechanism(s) and physiological importance of these nongenomic pathways are poorly understood, and as yet compounds that activate these processes at the expense of the better characterized genomic responses have not been developed. Considerably more is known about the mechanism(s) by which the genomic actions of SRs are manifest. Specifically, it has been determined that the ligand-free receptor is maintained in an inactive state in the absence of ligand through its association with a large heat shock protein (HSP) complex within the cytoplasm of target cells. Upon binding a ligand, the receptor undergoes a conformational change permitting the displacement of the

EXHIBIT H

HSP complex. This is followed by spontaneous receptor dimerization, nuclear translocation, and the subsequent interaction of the receptor dimer with the regulatory regions of target gene promoters. When occupied by an agonist, the promoter-bound receptor then recruits, in succession, functionally different classes of transcription coactivators that together effect a change in chromatin structure and enhance target gene expression. In the presence of an antagonist, the binding of corepressors to the SR is favored, and target gene expression is decreased (3). Based on these mechanistic insights, it is now believed that the cellular response to a specific SR ligand is determined by 1) the relative expression level in cells of receptor subtypes and isoforms; 2) the effect of the bound ligand on the overall shape of the receptor; 3) the effect of the adopted shape on cofactor recruitment; 4) the relative and absolute expression levels of individual cofactors in specific tissues; and 5) the activity of signaling pathways that impinge on the receptor-ligand complex (4–6). Much of this insight has come from the study of estrogen receptor (ER) pharmacology, where an explanation for the tissue selective agonist/antagonist activities of the selective ER modulator (SERM) tamoxifen was sought. Indeed, fueled by the clinical and commercial success of SERMs, there is now a heightened level of interest in using the insights obtained from the study of these compounds to develop tissue/process selective modulators of other members of this receptor family. The current study is aimed at defining aspects of the androgen receptor (AR) signal transduction pathway that are important in determining the pharmacological actions of androgens and how these may be exploited to develop selective AR modulators (SARMs).

Previous studies that have attempted to link the conformation of the AR-ligand complex and its pharmacological properties have focused mostly on the role of the interaction between the N- and C-terminal domains of AR (7–9). This approach was based largely on work that indicated that AR agonists, but not antagonists, are able to facilitate an interaction between the F/WXXLF motifs in the N-terminal domain of AR and the activation function (AF)-2 coactivator binding pocket located in the C-terminal ligand-binding domain (8, 10). Emerging from these studies was the tenet that an interaction between these domains was an obligate feature of AR agonists. However, it is the exception to this general rule that holds the most promise for the development of SARMs. Specifically, it has been observed that casodex and mifepristone (RU486), previously defined as AR antagonists, and partial agonists such as cyproterone acetate and medroxyprogesterone acetate, are unable to induce AR N-/C-terminal interactions, yet they exhibit various degrees of agonist activity in cell-based transcription assays (8, 11–13). It now appears more likely that N-/C-terminal interactions are involved primarily in the regulation of AR turnover and in determining agonist potency as a consequence of their ability to stabilize

ligand binding (13, 14). Thus, it remains to be determined how AR antagonists and partial agonists manifest agonist activity in some, but not all, cell and promoter contexts. We propose that AR partial agonists (SARMs) may function, as SERMs do on ER, by altering receptor structure in such a manner as to engender differential coactivator interactions, and that coactivator availability and activity determine ligand efficacy.

To test the SARM hypothesis, we sought to capitalize on the observation that the partial agonist activity of RU486 was mechanistically distinguishable from that exhibited by canonical AR agonists. In a previous report from our laboratory, we described the synthesis and characterization of compounds, Research Triangle Institute (RTI)-6413-018 (RTI-018) and RTI-6413-001 (RTI-001), which are similar in structure to RU486 but do not support AR N-/C-terminal interactions. However, these compounds possess full agonist activity in proliferation assays and display various degrees of agonist activity on classical androgen-responsive promoters (15). In the current study, we have built on these initial observations to probe the relationship between the conformation of AR induced by these compounds and their ability to regulate differential gene expression in prostate cancer cells. In this manner, we anticipated that we could test the SARM hypothesis and provide the mechanistic underpinning for screens to identify AR modulators with useful clinical properties.

RESULTS

Peptide Profiling Reveals Ligand-Dependent Changes in AR Structure

In the past, we have been able to monitor ligand-induced changes in ER structure using combinatorial peptide phage display, and we have used this technique to identify surfaces whose presentation is related specifically to the occupancy of the receptor by a specific ligand. Using this strategy, we sought to determine whether the distinct biological activities of RTI-001 and RTI-018 were related to their ability to induce distinct conformational changes in AR structure. A complete description of the phage display screening strategy that we have used has been described elsewhere (16). After affinity selection, the inserts of all phage that interacted with AR-RTI-001 in a specific manner were expressed as GAL4-DNA binding domain fusions and assessed for their ability to interact with a full-length wild-type (wt) AR-VP16 protein in a mammalian two-hybrid assay. The results of this assay, using three of the most informative peptides identified, are shown in Fig. 1A. The sequences of the peptides used in these experiments are shown in Table 1. Notably, all three peptides interact to a significant degree with AR in the absence of ligand and in the presence of antagonist Casodex. Treatment of cells with either RTI-001 or RTI-018, but not with ago-

EXHIBIT H
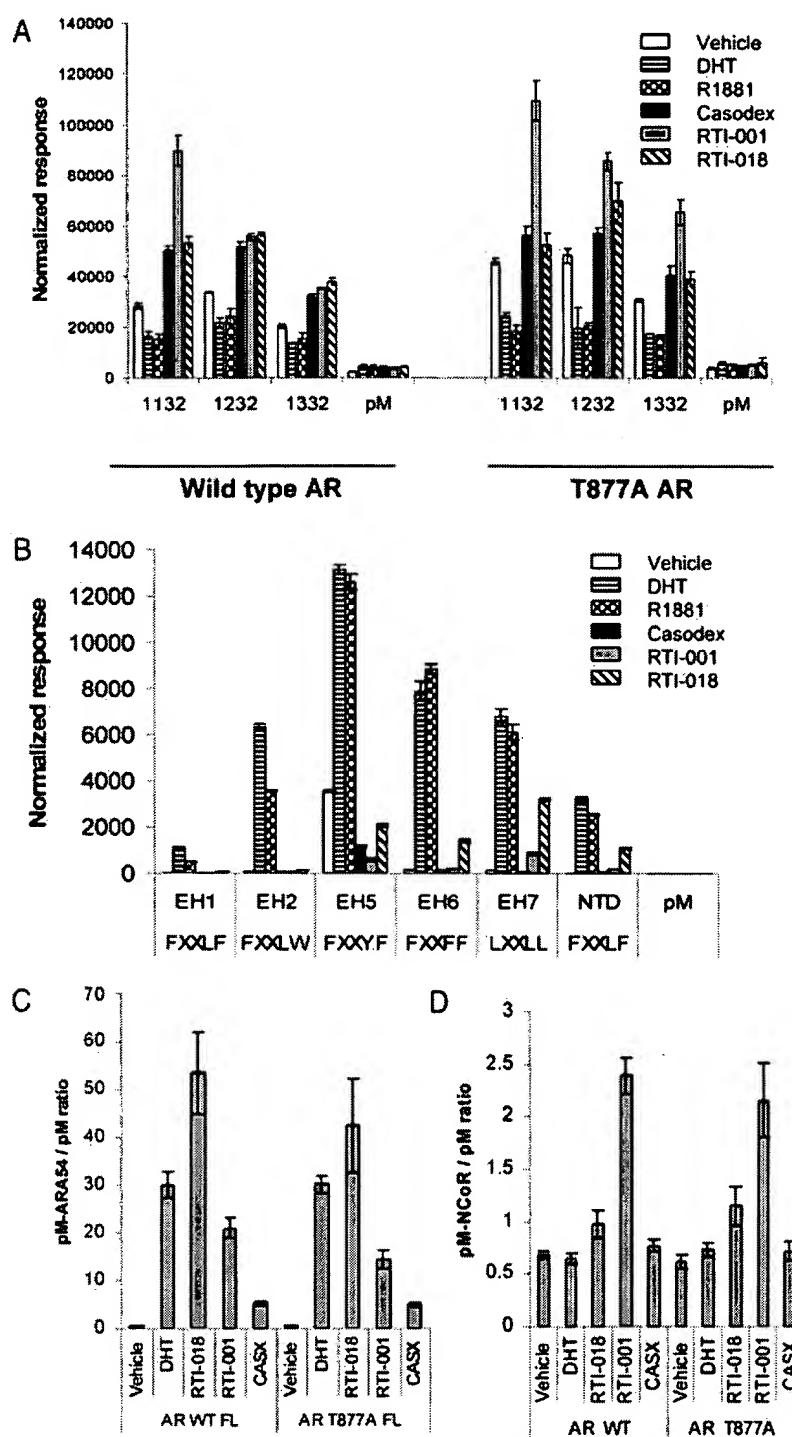
Fig. 1. Binding of Affinity-Selected Peptides and Known Cofactors to AR Liganded with Canonical Agonists and the SARM Compounds

Mammalian two-hybrid analysis was performed in HepG2 cells transfected with VP16-AR and peptide or cofactor fragments fused to Gal4-DBD as indicated. After 20 h, cells were treated in triplicates with hormones as indicated for 40 h. The peptide or cofactor interaction with the receptor was assayed using a luciferase reporter gene regulated by five copies of the GAL4-responsive element. Luciferase activity was normalized to β-galactosidase activity derived from the pCMV-βGal vector included with all transfections. A, Binding of the peptides selected in the presence of RTI-6413-001 to wt and T877A AR. pM, Gal4-DBD alone without peptide as negative control. B, Binding of the peptides selected in the presence of R1881. EH peptides were identified by Hur *et al.* (17). The sequence of the NTD peptide is derived from the sequence of human AR (CAI43080). C and D, Binding of fragments of known cofactors ARA54 (361–474 fragment) and C-terminal domain of NCoR (amino acids 1944–2453) to wt and T877A AR. The data in panels C and D are plotted as a ratio of the (VP16-AR/pM-cofactor) specific signal to the (VP16-AR/pM control) background. CASX, Casodex.

EXHIBIT H

Table 1. The Sequences of Peptides Used in the Mapping of the AR Surfaces in the Presence of SARMs

Peptide Name	Type	Sequence	Reference
1132–4	LXXLL	LQMWEKY<u>L</u>PA<u>LL</u>TMDDHVV	This report
1232–6	CoRNR	YY<u>L</u>SQW<u>HL</u>RGN<u>I</u>YDKISTVPTPS	
1332–4	X6-P-X6	LFHLRY<u>P</u>WLWDME	
NTD	FXXLF	SKTYRGAFQNLFQSVREVI	hAR (CAI43080)
EH1	FXXLF	SSRFESLFAGEKESR	(17)
EH2	FXXLW	SSKFAALWDPPKLSR	
EH5	FXXYF	SSNTPRFKEYFMQSR	
EH6	FXXFF	SRFADFFRNEGLSGSR	
EH7	LXXLL	SSRGLLWDLLTKDSR	

Constrained residues in peptides 1132–4, 1232–6, and 1332–4 are *underlined*. hAR, Human AR.

nists 5-α-dihydrotestosterone (DHT) or R1881, facilitates this interaction. Because the peptides were selected using RTI-001-liganded AR as a target, it was not surprising that some were found to bind with less avidity to the RTI-018-occupied receptor in mammalian two-hybrid assays. We also noted that the interaction of these peptides with AR in the presence of SARMs depends on the presence of both N-terminal domain and ligand binding domain (LBD) because neither of these domains is able to recruit these peptides (data not shown). Interestingly, the canonical agonists DHT and R1881 discouraged the binding of these peptides to AR. Although the screening was performed using wt AR as a target, we have demonstrated in Fig. 1A that the selected peptides display the same binding characteristics when assessed on the T877A AR, the receptor mutant expressed in LNCaP cells. For these studies, we also created additional GAL4 peptide fusions using the AR AF-2 interacting FXXLF-containing peptides identified recently by Hur *et al.* (17) using phage display of DHT-activated AR LBD. For comparative purposes, we also evaluated a similarly sized peptide fragment containing the native FXXLF derived from the N-terminal domain of AR, which is responsible for the intra- or intermolecular interaction of the AR amino and carboxyl termini. As expected, all of these FXXLF-containing peptides interact with AR in mammalian two-hybrid screens in the presence of either DHT or R1881 (Fig. 1B). However, the binding patterns observed in the presence of the two SARMs are quite distinct. In the case of EH1, EH2, and EH5, for instance, both SARMs function like the antagonist casodex. The peptides EH6, EH7, and N-terminal domain (NTD), on the other hand, are able to interact, at least partially, with AR in the presence of RTI-018. The inability of RTI-001 to facilitate these interactions provides compelling evidence that the structures of AR in the presence of these SARMs are similar but distinct. These peptides interact with T877A AR in an identical fashion (not shown).

The peptide profiling assays revealed distinct structural changes in AR associated with the binding of different ligands. However, because of the complexity of the peptide libraries we have generated exceeds that of the human genome, it was unclear whether the

conformational differences induced by these ligands would be sufficient to elicit differential cofactor interactions. To address this issue, we again turned to the mammalian two-hybrid assay and evaluated the interaction of AR with the receptor-interacting domains of validated AR-cofactors. Given the fact that the best characterized cell culture-based model of prostate carcinoma, LNCaP, bears a mutation in AR LBD (T877A), we also tested whether this mutation affects the recognition of these cofactors in the mammalian two-hybrid assay. It became evident from these studies that both SARMs stimulate the recruitment of the FXXLF-containing fragment of ARA54 to AR, although we reproducibly observe a more robust interaction with the RTI-018-activated receptor (Fig. 1C). In contrast, the binding of the receptor interacting domain of the corepressor nuclear receptor corepressor (NCoR) was only observed in the presence of RTI-001 (Fig. 1D). Interaction of both coactivator and corepressor fragments with AR was dependent on the presence of the N-terminal domain because we could not detect any interaction with AR LBD (AR 624–919) alone (data not shown). We believe that this represents an inherent instability in the LBD of AR rather than an indication that the amino terminus of the receptor contributes directly to the peptide binding surface. Importantly, we did not observe any differences in the recruitment of these two cofactors in the presence of different ligands between wt and T877A AR. Given these data, it is reasonable to expect that DHT- and SARM-activated AR will have overlapping, though distinct, biological activities and similarly, that in some biological systems RTI-001 and RTI-018 will be distinguishable.

Ligand-Regulated Changes in AF-2 Architecture

Recent crystallographic studies have provided considerable insight into the mechanisms by which coactivator peptides interact with the AR AF-2 when the receptor is occupied by an agonist (17, 18). The key residues involved in the formation of the peptide binding site are illustrated in Fig. 2A. Given the peptide and cofactor binding data, and the N-/C-terminal interaction data, we hypothesized that the SARMs RTI-001 and RTI-018 may alter the conformation of the AF-2 pocket in a manner distinguishable from that observed

EXHIBIT H

Area, Å²

	DHT	RTI-6413-018	RTI-6413-001
WT	475	527	619
T877A	509	545	615
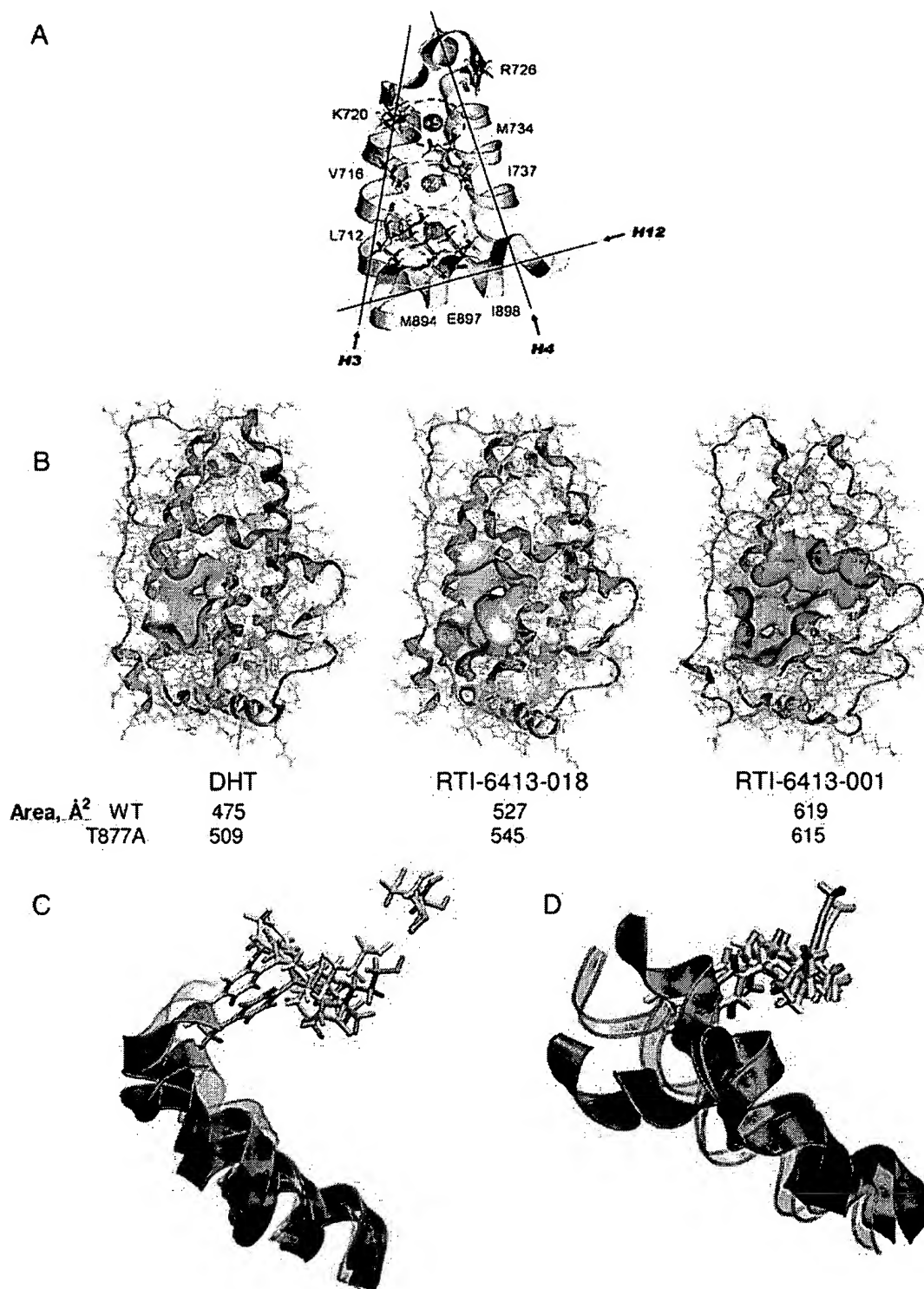
Fig. 2. Computed Structural Alterations within the AF-2 Site upon SARM Binding

A, The structure of the AR AF-2 (1I37) site, showing the key residues involved in the formation of the peptide-interacting surfaces. B, Solvent-exposed area of AF-2 (coactivator peptide binding site) pocket. Residues included in surface area calculations: L712, V716, W718, M734, I737, W747, M894, M895, I898. The *numbers below the structures* show the calculated solvent-accessible area of AF-2 in both wt and T877A AR variants. WT (wt) structures shown. C and D, Predicted repositioning of the helix 12 in the wt and T877A AR in the presence of DHT, RTI-018, and RTI-001. C, Calculated positions of H12 in the wt (*purple ribbon*) and T877A (*red ribbon*) in the presence of RTI-018. Position of H12 in the presence of DHT (wt AR) is shown in *translucent gray*. D, Calculated position of the H12 in wt and T877A AR in the presence of RTI-001. Color coding is the same as in panel C. RTI ligands are shown and color coded as follows: in the context of wt AR, *green*; in T877A AR, *yellow*. Position of Ser 778 is shown in panel C and color coded the same as ligand.

EXHIBIT H

in the presence of DHT. As a first step in testing this hypothesis, we performed a molecular dynamics (MD) simulation of AR complexed with the RTI ligands and DHT and compared the resulting structures. Because LNCaP cells, which were used for a number of experiments presented in this manuscript, express the T877A AR mutant with altered ligand specificity, we used both wt and T877A structures for molecular modeling experiments. For the MD simulations, the initial relative positions of the RTI-001 and RTI-018 ligands were generated by superimposing the steroid core of the RTI ligands over the steroid core of DHT, followed by removal of the DHT molecule. The structures with DHT, RTI-018, and RTI-001 were then minimized and equilibrated. MD simulations were performed for 1 nsec. After equilibration, MD trajectories were analyzed for the conformational differences between DHT- and SARM-bound receptor.

One important indication of a conformational change in AF-2 is the modification of the solvent accessible area of the residues that comprise the AF-2 pocket. Thus, solvent accessible areas were calculated for the hydrophobic residues in the AF-2 pocket and averaged over MD trajectory snapshots. The results of this analysis indicate that the solvent accessible area of the AF-2 pocket on the surface of the receptor is larger in the presence of RTI-018 than in the presence of DHT, and is even larger in the presence of RTI-001 (Fig. 2B). We extended these analyses to quantitatively estimate the observed alterations in the AF-2 shape. To do this, we measured the distances between pairs of residues (Cβ atoms) that previously have been shown to form the pocket that can accommodate the +1, +4, and +5 residues of an FXXLF motif in the simulated structures of AR LBD in complex with DHT or SARMs. The measurements, averaged over the MD trajectory, are shown in Table 2. In these estimations, we assumed that the distances between 1) M734-K720 defines the size of +5 pocket, 2) I737-V716 and I737-L712 define the size of the +5 and +4 pockets, 3) I737-I898, and I737-M894 are related to the size of +1 pocket, and I737-E897 and K720-E897 define the relative positions of the charge clamp residues of AF-2. It becomes evident from Table 2 that in the AR (both wt and T877A)-RTI-018 complex the conformation of AF-2 is similar to that in AR-DHT

complex, with the exception of the +4 to +1 region in wtAR-RTI-018 complex, which is described by the I737-L712 distance. This distortion may be responsible in part for the observed lower transcriptional activity of wtAR-RTI-018 compared with T877A AR-RTI-018 in transfected cells (data not shown) because it was found to differ significantly between the two receptors (12 Å *vs.* 9.9 Å). It should be noted that we observed an increase of predicted distances between all residues in H12 and corresponding reckoning points elsewhere in AF-2 in T877A AR-DHT *vs.* wtAR-DHT, indicating a possible lateral shift of H12 in the mutant AR by approximately 1.5 Å. However, wt and T877A ARs demonstrate equal ability to activate transcription with DHT in transfected cells (data not shown).

The largest distortion observed within the AF-2 pocket occurs upon binding RTI-001 and is located in the area that accommodates the +1 residue in the coactivator peptides. Specifically, we observed that the distance between the charge clamp residues K720 and E897 increases dramatically in the case of both wt and T877A AR (by 4.3 and 3.4 Å, respectively). The distances describing the shape of +1 pocket and the configuration of H12 were also calculated to be substantially different in RTI-001 complexes compared with DHT. This indicates a possible change in the position and shape of H12 and is different from the alteration predicted for the RTI-018 complex. Also, it becomes apparent from Table 2 that the shape of H12 is altered differently in wt and T877A-RTI-001 complexes (I737-M894 distance).

The model presented in Fig. 2, C and D, represents the predicted conformations of H12 in the presence of the RTI ligands in both wt and T877A contexts. The chemical structures of the ligands are shown in Supplemental Fig. 1, which is published as supplemental data on The Endocrine Society's Journals Online web site at http://mend.endojournals.org. As can be seen, RTI-018 causes little change in the position of H12, in both wt and mutant receptors (Fig. 2C). In both cases, its configuration was predicted to be similar to that of the AR-DHT complex. In the case of RTI-001, the configuration of H12 is altered dramatically, for both wt and mutant AR. The differences between the structures of AR-SARM complexes are determined by the

Table 2. Interatomic Distances (Å) between the Key Residues in the AF-2 Pocket of AR as Measured for the MD Trajectory Snapshots and the Original DHT-AR Structure [1I37 (27)]

Residues	DHT		RTI-6413-018		RTI-6413-001	
	WT	T877A	WT	T877A	WT	T877A
Met734-Lys720	10.5	11.2	10.05	11.1	12.0	10.1
Ile737-Leu712	9.1	9.2	12.02	9.9	9.1	9.9
Ile737-Val716	5.9	5.8	5.8	6.5	7.3	5.7
Ile737-Ile898	8.15	10.0	9.5	11.0	12.8	16.0
Ile737-Met894	12.6	13.9	12.3	13.0	10.4	16.1
Ile737-Glu897	12.5	14.0	12.6	14.5	14.3	15.5
Lys720-Glu897	18.9	20.0	19.5	21.2	23.2	23.4

EXHIBIT H

positioning of the ligand within the ligand-binding pocket. In the wt context, the RTI ligands are predicted to make a hydrogen bond between 17β-acetyl and the T877, in a manner similar to DHT. This allows the anchoring of the 17-position and the fixation of the steroid core in the ligand-binding pocket in a position similar to that of DHT. In the mutant AR context, however, this hydrogen bond to the steroid core is absent, which allows for the drift of the ligand within the pocket. However, in the case of RTI-018, this drift is limited due to the predicted hydrogen bond between the hydroxyl group of the 17-α-propan-3-ol and the backbone oxygen of serine 778. As a result, the RTI-018 ligand is predicted to assume a position in which the bulky 11β substituent is positioned away from the helix 12 and is not making physical contact with it. This allows for the preservation of the agonist-like conformation of the helix 12. However, the positioning of the 11β-p-acetylphenyl in the wt receptor was observed to be in a closer proximity to helix 12, causing a partial degradation of its native structure, which may be responsible for the lower efficacy of RTI-018 on wt AR in transfected cells (Fig. 2C and Supplemental Fig. 2). RTI-001, unlike RTI-018, features the 17α substituent that is unable to form a hydrogen bond. In the wt context, this ligand is predicted to form a hydrogen bond with T877 through the 17β acetyl oxygen, which results in the direct physical contact between its 11β-dimethylaniline group and the base of helix 12. This results in the unwinding of the proximal region of helix 12, and substantial changes to the structure of AF-2, which involve M895, M896, and charge clamp residue E897 (Fig. 2D). In the T877A context, the hydrogen bond that fixes the 17-position of the steroid core is absent, which allows for the shift of the ligand molecule within the ligand binding pocket. The predicted new position of the RTI-001 ligand places the 11β substituent on the opposite side of the base of the helix 12, but still in direct contact with it. The resulting structural alterations in the Helix 12 in the T877A context are different from those observed in the wt receptor. The main differences are that, unlike the wt receptor, for which the largest distortions were observed in the proximal region of the helix, in the T877A, we observed a planar shift of the entire helix 12 away from AF-2 pocket (Fig. 2D). This results in the increased distances between the charge clamp residues and is predicted to negatively affect the transcriptional activity of the receptor.

We conclude from these findings that the subtle change in the substituents at the 11β and 17α positions has a dramatic impact on the structure of the AF-2 and coactivator peptide binding preferences. Intuitively, these structural rearrangements would be predicted to have an immediate impact on the transactivation properties of these compounds, making RTI-001 a weaker agonist than RTI-018 and DHT. As will be shown in the next section, these predictions were borne out when the functional properties of these

ligands were compared in relevant models of AR action.

Linking Ligand-Induced Changes in AR Structure to Differences in Gene Expression Profiles

A key step in proving the SARM hypothesis relies on the ability to establish a link between AR structure, gene expression, and specific biological activities. To achieve this, we chose to use Affymetrix Gene Chip technology (Santa Clara, CA) to survey genome-wide changes in AR-dependent gene transcription in the presence of different ligands in LNCaP cells. For these initial studies, we compared DHT- and RTI-018-induced changes in mRNA levels after 6 and 24 h of hormone treatment. We also performed independent follow-up experiments where the activities of RTI-018 and RTI-001 on a select number of genes were compared. To establish a baseline, we used the profiles observed in cells treated with vehicle alone. Using a mixed linear statistical model on the log2 perfect-match data along with a Bonferroni correction to control the probability of one or more false positives at 0.05, a total of 1433 significantly changed genes and expressed sequence tags (ESTs) were identified on the Affymetrix HU133 A chip, and an additional 296 were detected on the B chip. A cluster analysis of the significantly altered genes revealed two major expression profiles, the characteristics of which are described in detail below (Fig. 3). The first class (cluster 1), which contains 747 genes and ESTs, includes those genes whose transcription is repressed by androgens. For the majority of these genes, transcriptional repression became evident at 6 h and continued for 24 h or more. Interestingly, for most of these genes maximal repression by DHT was evident at 6 h, with little additional repression occurring in the subsequent 18 h. However, in the presence of RTI-018, transcriptional repression increased over time, so that by 24 h the magnitude of repression became significantly greater than that observed with DHT treatment. For some genes from this cluster, however, both DHT and RTI-018 displayed nearly equal efficacy of repression at 24 h. Examples of both kinds of regulation of genes from this group are presented in Fig. 4 and include the 3-hydroxymethylglutaryl coenzyme A (CoA) synthase 2 (HMGCS2, NP_005509) and the ATP-dependent transporter G (ABCG1, NP_004906). The ability of the antagonist casodex to inhibit RTI-mediated repression confirmed that this repression is AR dependent.

Most of the AR-responsive genes identified were positively regulated to some degree by DHT and both SARMs (Cluster 2; Fig. 3). These genes fell into two groups: 1) those whose expression was up-regulated at an early time point (6 h), and 2) genes that were up-regulated at a later (24 h) time point, whereas lower or no induction was observed at 6 h time point. Two genes from this class, SLC16A6 (NP_004685) and Kallikrein-3 (PSA, NP_001639), were selected for a more complete analysis (Fig. 5). Both were significantly in-

EXHIBIT H
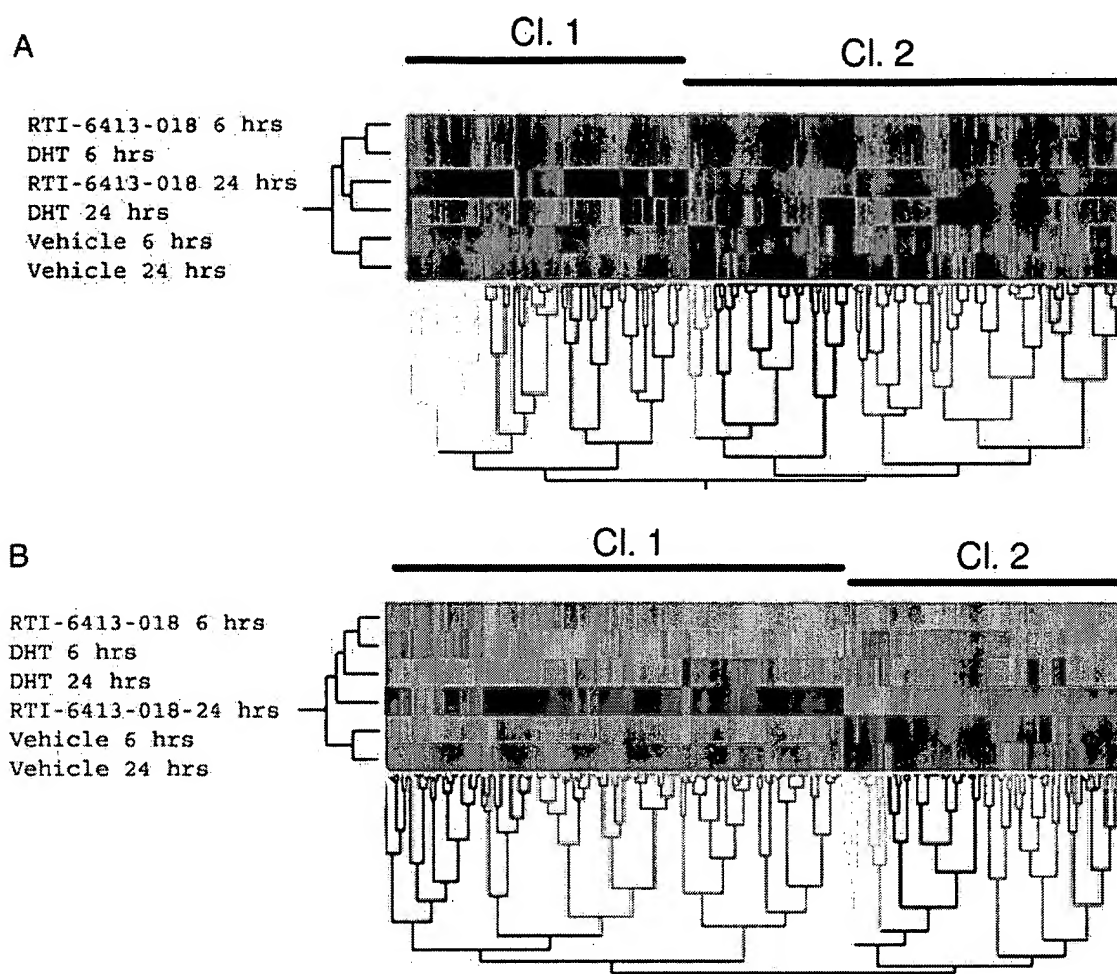
Fig. 3. Hierarchical Clustering Analysis of DHT and RTI-6413-018-Regulated Genes in LNCaP Cells

Clustering analysis of 1430 significant genes and ESTs on chip A, and 297 significant genes and ESTs on chip B (Affymetrix Hu.133 chip set) is shown. *Red* and *blue* depict deviations in normalized, standardized mean intensity from the average intensity across the treatment conditions, up and down, respectively. Two major groups of genes showing common regulatory behavior are indicated: cluster 1 (Cl.1), down-regulated by androgens; cluster 2 (Cl.2), up-regulated.

duced by DHT and RTI-018, but the latter compound demonstrated lower efficacy and potency. However, overall analysis of the 388 genes from this cluster on the HG-Hu133-A chip suggests that, on average, RTI-018 acts as full agonist at 0.1 μM. When analyzed in a similar manner, RTI-001 functioned as a weaker partial agonist. The agonist activity of all three compounds was attenuated by inclusion of the antiandrogen casodex. Casodex shows little inhibition at 6 h, which could be partially enhanced by preincubation of cells with casodex before the addition of hormones. However, the improvement is not significant, which is in agreement with the notion that casodex acts as a low-affinity competitive antagonist (Supplemental Fig. 3, A–C). As can be seen in Fig. 5, A and B, and in Fig. 3, some genes demonstrate a right shift in DHT potency between 6 and 24 h. The magnitude of the loss of potency of DHT varies depending on the cell passage and other as yet unknown factors. DHT does not inhibit gene activation by RTI-018 at 24 h, which ex-

cludes the possibility of the conversion of DHT into an antagonistic derivative as a reason for the loss of potency of DHT response over time (Supplemental Fig. 4). We cannot exclude the possibility, however, that this right shift is caused by degradation of DHT into inactive metabolites. This, however, seems unlikely, given the fact that hundreds of genes show response at 24 h to DHT. It would appear, therefore, as if members of this class of genes are under some type of negative feedback control that alters sensitivity to hormones, and that the RTI-SARMs do not induce this activity. Currently, we are trying to define the molecular mechanism(s) that regulate ligand potency and/or kinetics of activation on these genes. Cycloheximide inhibition studies revealed that most of the tested genes require continuous protein synthesis for expression (data not shown). Therefore, it cannot be excluded that even for the down-regulated genes, the primary effect of androgens is up-regulation of an upstream effector. Interestingly, we observed a 100% overlap between the

EXHIBIT H
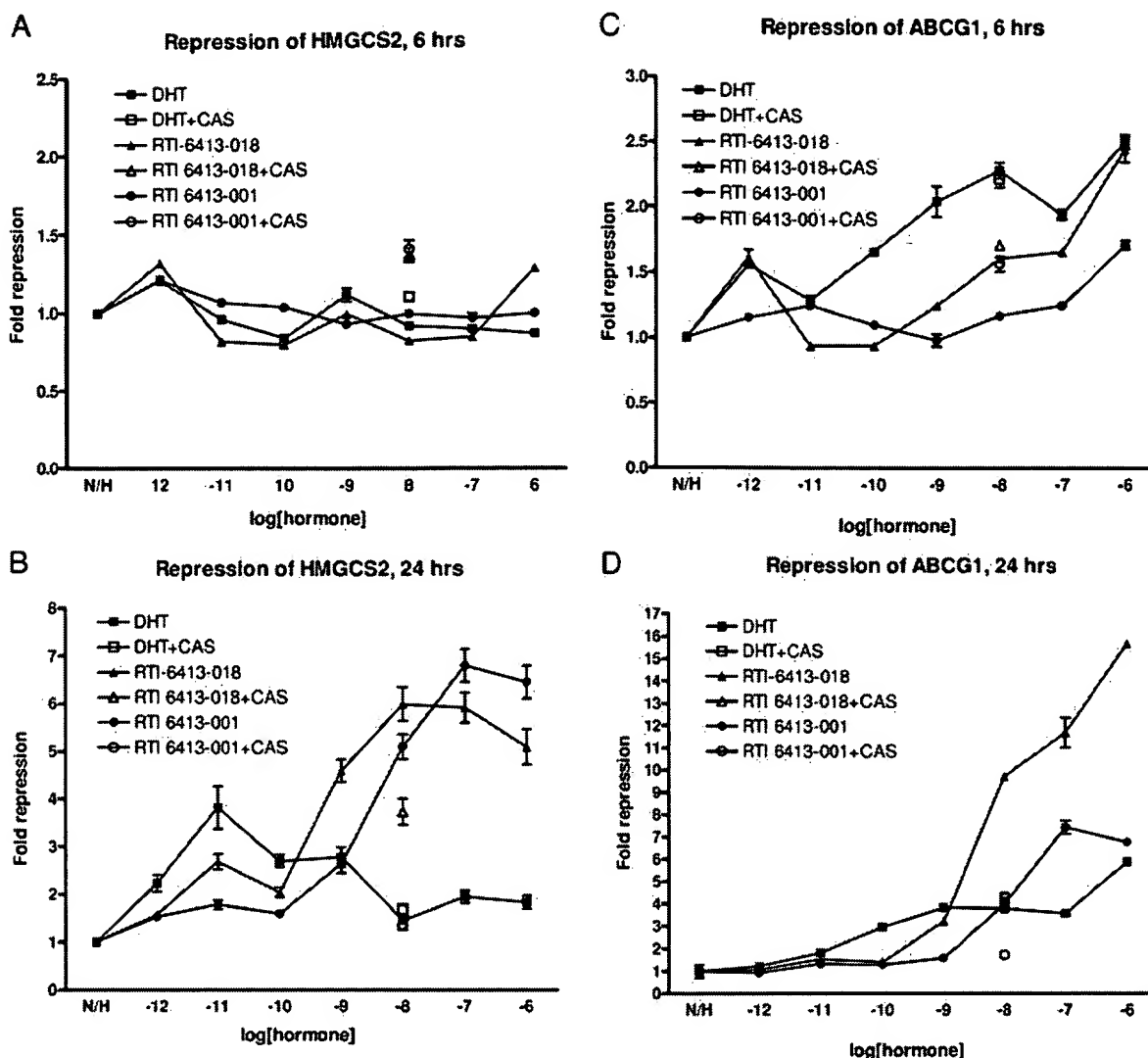
Fig. 4. Real-Time RT-PCR Analysis of the Dose-Response Patterns of Two Representative Genes that Are Down-Regulated by Both DHT and RTI-6413-018

ABCG1 and HMGCS2 genes are shown. Both genes appear to be more strongly repressed by RTI-018 and RTI-001 than by DHT. *Error bars* show SEM. Casodex was used at 1 μM. The hormone plus casodex points shown correspond to 10 nM hormone competed with ×100 molar excess of casodex. N/H, No hormone.

spectra of DHT- and SARM-regulated genes. The differences between compounds, therefore, lie not in the altered promoter specificity, but in altered kinetics of the response. A more complete list of the representative genes from each cluster is presented in Supplemental Table 1. The Affymetrix pivot tables are included in the supplemental materials.

In summary, our peptide profiling and modeling studies predicated that DHT and the chosen SARMs should be biologically distinguishable, a finding that was borne out in the analysis of the gene expression profiles in cells treated with these compounds.

Classification of the Regulated Genes

Although the gene array data provided important endpoints with which to study and classify androgens, we also wished to determine whether there is an association between the classes of regulated genes and specific biological responses. To achieve this, we expanded our studies to use standard annotation algorithms for the androgen-regulated genes from the three classes described above. We performed a gene ontology analysis using the 960 regulated unique genes with known functions that we identified in our array studies. The assignments arrived at from this study are as follows, the numbers *in brackets* indicating the number of genes assigned to each category: 1) cell cycle control [30], 2) DNA metabolism [36], 3) cellular metabolism [76], 4) cell maintenance and homeostasis [221], 5) signal transduction [97], 6) regulation of apoptosis [14], 7) mitochondrial maintenance and energy metabolism [36], and 8) transcription fac-

EXHIBIT H
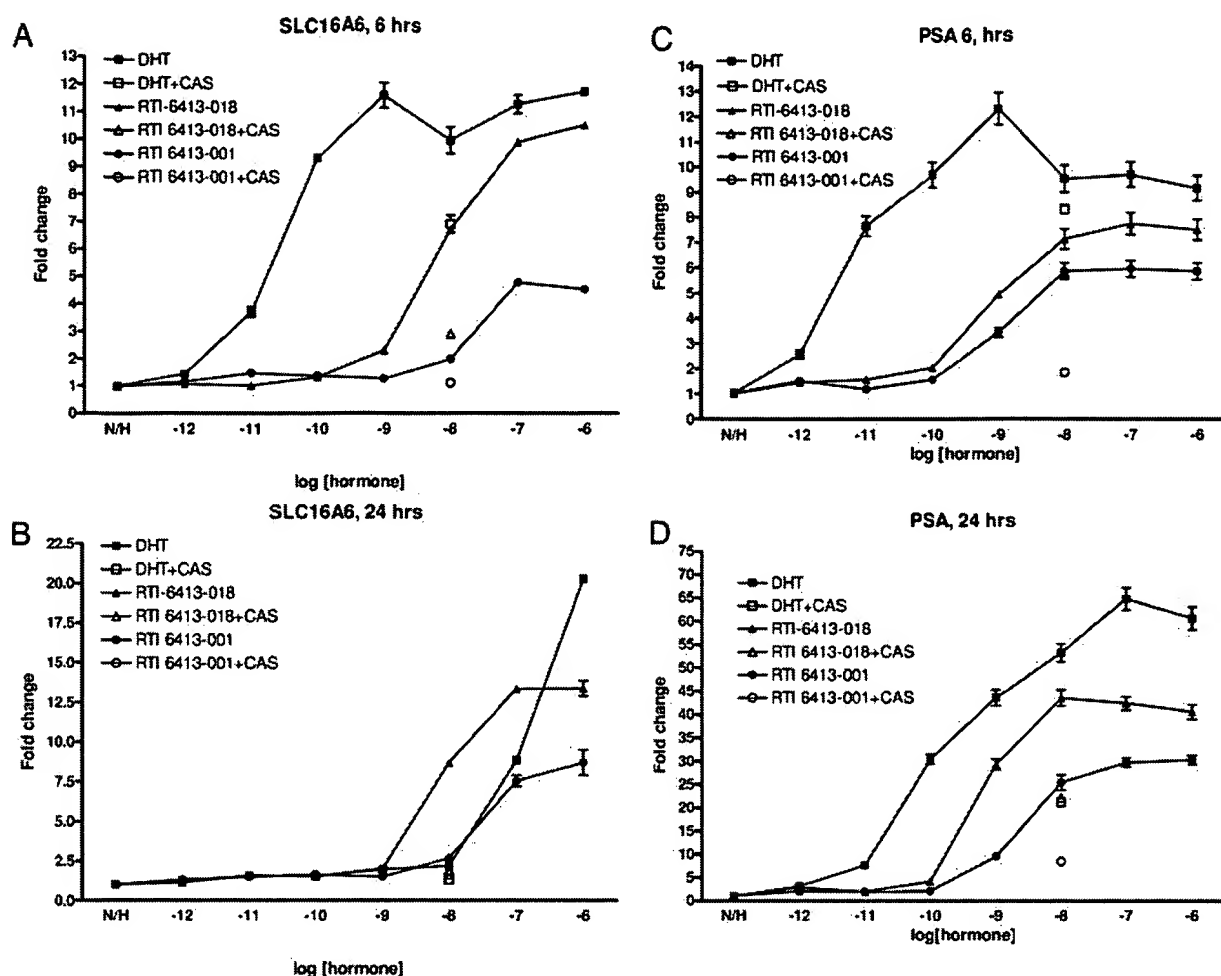
Fig. 5. Real-Time RT-PCR Analysis of the Time- and Dose-Response Patterns of Two Representative Genes that Are Up-Regulated by DHT and SARMs.

SLC16A6 and PSA (KLK3) are shown. Consistent with the placement of these genes in the hierarchical clustering analysis, SLC16A6 shows transient up-regulation by DHT and more prolonged up-regulation by SARMs. PSA (prostate-specific antigen), similar to other genes from its cluster (late up-regulated) shows dramatic increase in mRNA level between 6 and 24 h. *Error bars*, SEM. Casodex was used at 1 μM. N/H, No hormone.
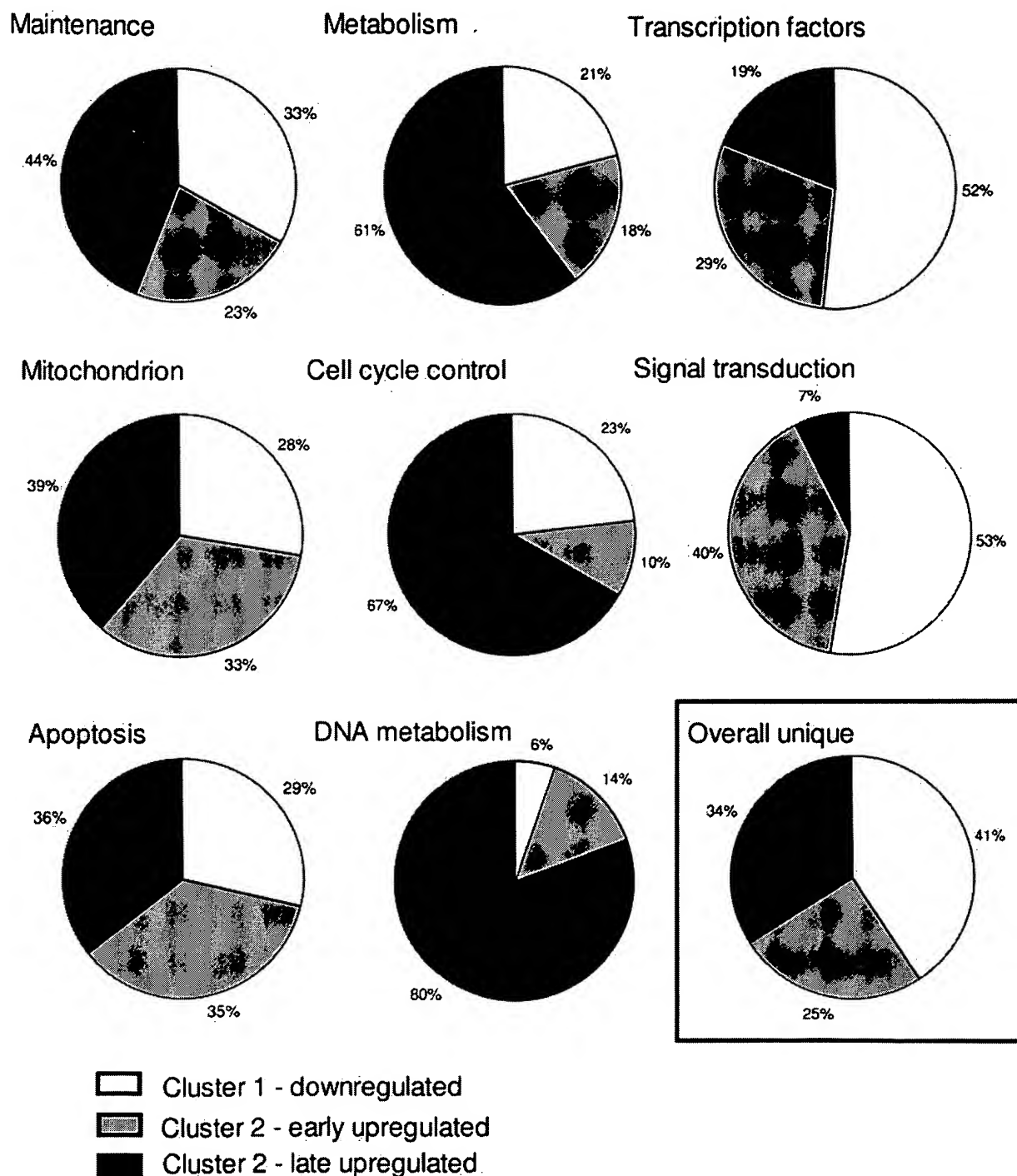
tors [68]. A total of 578 genes were assigned to one of the above categories. Next we assessed the distribution of genes from each gene ontology group among the main classes of coregulated genes identified in our analysis above (Fig. 6). Considering all of the genes identified, it is apparent that each class of regulated genes (down-regulated, early up-regulated, and late up-regulated) is represented to a similar *degree (lower right panel)*. Likewise, each class is represented to the same degree among genes associated with mitochondrial biogenesis and function, cell maintenance, and regulation of apoptosis. It is noticeable, however, that a significant number of genes involved in metabolism, cell cycle control, and DNA metabolism, belong to the class of late up-regulated genes. Indeed, 61% of genes involved in metabolism, 67% in the control of cell cycle group, and 80% in the DNA metabolism group are up-regulated at the late (24 h) time point. In contrast, genes from this class are underrepresented in the transcription factors and signal transduction

groups, comprising only 19% and 7% respectively (Fig. 6). Interestingly, in these groups, it is class 1, the down-regulated genes, which are represented most frequently. It should be noted that part of the observed pattern of gene regulation could be attributed to the T877A mutation in LNCaP AR, which alters ligand specificity, or to other cellular factors specific to this cell line. Similar studies performed in prostate carcinoma LAPC4 cells, which harbors wt AR, demonstrated a significantly different pattern of regulation of representative genes from each class (Supplemental Fig. 5).

Different Physiological Pathways Are Differentially Regulated by the Candidate SARMs and Canonical Agonists

It is clear from the studies presented above that RTI compounds do not act simply as partial agonists but display differences in the gene activation kinetics.

EXHIBIT H

Maintenance

33%
44%
23%

Metabolism

21%
61%
18%

Transcription factors

19%
52%
29%

Mitochondrion

28%
39%
33%

Cell cycle control

23%
67%
10%

Signal transduction

7%
40%
53%

Apoptosis

29%
36%
35%

DNA metabolism

6%
14%
80%

Overall unique

34%
41%
25%

☐ Cluster 1 - downregulated
▨ Cluster 2 - early upregulated
■ Cluster 2 - late upregulated

Fig. 6. Gene Ontology Classification of the Known Androgen- and SARM-Regulated Genes
  The 578 of 960 regulated genes with known functions were classified according to their gene ontology annotation terms as indicated. Within each gene ontology group, genes were classified according to their regulation pattern. The *lower right panel* shows the distribution of all 578 genes among the three major regulation pattern groups.

Therefore, we became interested in testing whether this altered kinetics of gene activation results in differential regulation of physiological pathways which are known to be regulated by androgens. The two easily measured endpoints of androgen action in LNCaP cells are proliferation and accumulation of lipids in the cytoplasm (19). As reporter earlier, the RTI SARMs act as full agonists in proliferation assays (Fig. 7B). We therefore wished to test whether they would have the same or a different effect on lipogenesis. In the microarray analysis of the androgen- and SARM-responsive genes, we had also detected a number of genes

EXHIBIT H

A   Lipogenesis in LNCaP

B   Proliferation in LNCaP
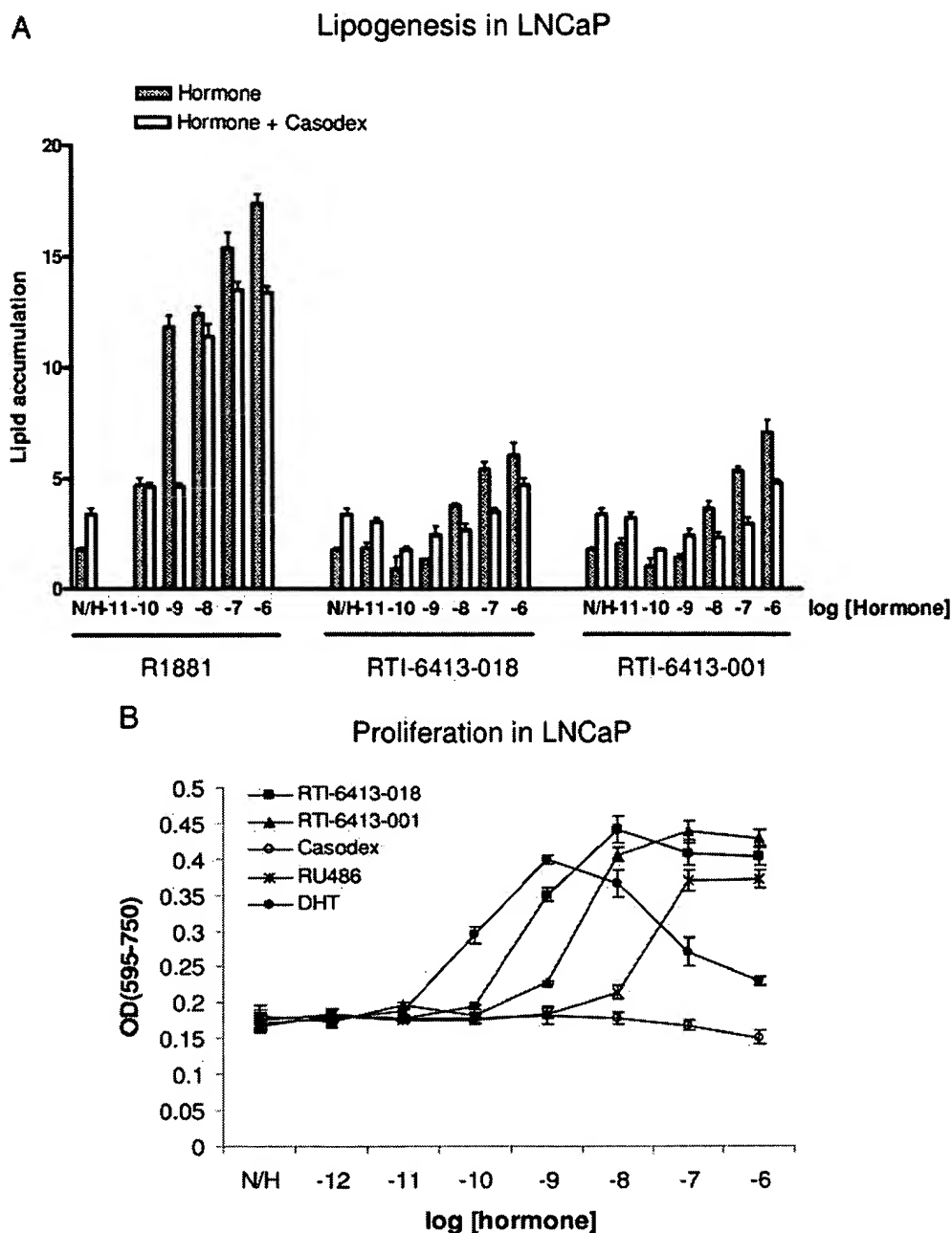
Fig. 7. Accumulation of Neutral Lipids in LNCaP Cells in Response to Androgen Treatment

A, Increased lipogenesis in LNCaP in response to androgens. Lipid accumulation over 72 h was measured by Oil Red O inclusion as described in *Materials and Methods*, and normalized to the total cell number. Casodex was used at 1 μM. B, Proliferation of LNCaP cells in the presence of SARM compounds. For proliferation assays, LNCaP cells were seeded at 80,000 cells per well in 24-well clusters and allowed to attach and spread for 3 d in medium containing dextran-charcoal filtered serum to reduce hormone background. Hormones were added on d 4 and the medium was refreshed on d 6 and 8. Cell growth was assayed on d 10 by DPA assay (36). N/H, No hormone.

that are involved in lipid metabolism, such as lipoprotein lipase, low-density lipoprotein receptor, insulin-induced gene 1, stearoyl-CoA desaturase δ9, stearoyl-CoA desaturase δ5, ABCG1, emapomyl binding protein, DHCR24 (Seladin-1), fatty aldehyde dehydrogenase, carnitine O-ocanoyl transferase, HMG-CoA reductase, HMG-CoA synthases 1 and 2, fatty acid synthase, and others. Most, but not all, of these genes

belong to the class of late up-regulated genes, and are induced by both DHT and SARMs, with SARMs acting as full or partial agonists. Fatty aldehyde dehydrogenase and carnitine O-ocanoyl transferase belong to the class of early up-regulated genes, whereas ABCG1 and HMGCS1 belong to class 1 (late down-regulated). Most of these genes show a pattern of regulation by SARMs different from that by DHT. We

assessed the net effect of the coordinated expression of these and other genes involved in the regulation of lipid metabolism by measuring the lipid content of LNCaP cells after treatment with the canonical agonists and the RTI compounds. Surprisingly, accumulation of neutral lipids in the presence of either SARM is minimal compared with that observed in the presence of the nonmetabolizable AR agonist R1881 (Fig. 7A). Measurable accumulation is observed only at concentrations above 10 nM, and even at micromolar concentrations there is only minimal production of lipids. This is in contrast to the high efficacy of these compounds in proliferation assays, where they stimulate proliferation as well as canonical AR agonists. These results indicate that candidate SARM compounds are able to differentially regulate distinct physiological pathways in LNCaP cells. Given the moderate sensitivity of lipid accumulation to the inhibition by casodex, it remains to be determined whether the lipogenesis in LNCaP cells is mediated solely through AR, or there is an involvement of other nuclear receptors, such as PPARα.

DISCUSSION

With the development of SERMs and their successful introduction into the clinic, there has been a high level of interest in exploring the possibility of developing selective modulators of other ligand-regulated nuclear receptors. In this regard, it is clear that tissue- or process-specific modulators of the progesterone receptor, glucocorticoid receptor, and AR would have tremendous clinical utility. Examples would be selective progesterone receptor modulators that separate activities in the breast and uterus; selective glucocorticoid receptor modulators by which the metabolic, osteopenic, and antiinflammatory activities could be separated; and finally SARMs that separate the anabolic action of classical androgens from their negative effects on prostate, central nervous system, and lipids. Although the advent of SERMs provided the impetus to embark on a search for modulators of these receptors, it has until recently been unclear how this could be accomplished. The discovery of SERMs was fortuitous in that the first member of this class, tamoxifen, was initially characterized as an ER antagonist but was subsequently found to have antiresorptive activities in bone (20). The second SERM raloxifene (formerly known as keoxifene) was also developed as an ER antagonist but differed from tamoxifen in that it did not display uterotrophic activity (21–23). Although these SERMs were discovered serendipitously, the subsequent insight into their mechanism of action has led to the development of more SERMs and selective modulators of other nuclear receptors. Specifically, it has become clear that different ligands have different effects on ER structure and that these differences have distinct biological consequences (24). It was within the

framework of this understanding that we began our study on the development of SARMs. Here we present the demonstration that: 1) AR structure is influenced by the nature of the bound ligand; 2) the conformational changes observed are likely to be important as they lead to the presentation of different protein-protein interaction surfaces; 3) these conformational changes track with differential regulation of gene expression; and 4) with specific biological activities. The ability to alter AR structure and thus effect different biological responses raises expectations that androgens with favorably dissociated activities with clinical utility will be identified.

The candidate SARM compounds used in our studies are all derived from the core structure of RU486, a drug with demonstrated AR partial agonist activity (12). This compound belongs to a class of nuclear receptor antagonists that contain a bulky side chain at the 11β position that functions by displacing helix 12 in the coactivator binding pocket of the LBD of the receptors with which it interacts (25). We introduced changes into the structure of RU486 and assessed the impact of these changes on the conformation of AR and the resulting impact on downstream biology. Interestingly, we discovered that a simple replacement of a 17β hydroxyl group in RU486 with an acetyl moiety (RTI-6413-001) leads to increased proliferative activity in LNCaP cells, which is likely to have resulted from the increase in ligand affinity (Fig. 7B). Importantly, the transcriptional agonist activity of the resulting compound remains low in reporter assays and in assays where the transcription of endogenously expressed AR-responsive genes was assessed. The replacement of the 11β-p-dimethylaniline and 17α-prop-1-yne groups with 11β-p-acetylphenyl and 17α-propan-3-ol moieties yielded the compound RTI-018. Like RTI-001, this compound functions as a full agonist in proliferation assays, and a partial agonist in cell-based transcription assays. It should be noted that the agonist activity of these compounds, both in proliferation and transcription assays, occurs in the absence of a detectable N-/C-terminal interaction. Similar characteristics were reported for a series of 11β-alkyl analogs of RU486 in which the length of the alkyl side chain was correlated with AR affinity, inhibition of N-C interaction, and partial agonist activity. Of interest, one of these compounds, 11β-pentyl-Δ^9-19-nortestosterone, does not support N-/C-terminal interaction, potently inhibits N-/C-terminal interaction induced by DHT, and shows appreciable partial agonist activity with IC_{50} in subnanomolar range and efficacy over 50% that of DHT (11). Together, these findings indicate that significant agonist activity of AR ligands can occur in the absence of a classical AF-2 coactivator-interacting pocket.

A central tenet of the SARM hypothesis is that it will be possible to modify AR structure with small molecules and that in doing so the genetic program regulated by this receptor can be modified. Our studies with the RTI compounds reveal that the gene expres-

EXHIBIT H

sion profiles overlap considerably with those of a classical AR agonist, although very significant differences in the kinetics of target gene induction were noted. Using combinatorial peptide phage display and molecular modeling, we have been able to demonstrate that these differences in response may be correlated to specific changes in AR structure in and around the AF-2 region of the receptor. We interpret these data to mean either that different surfaces are presented on the receptor upon binding different ligands, or that there are functionally important changes in a single pocket afforded by different compounds. The observation that the RTI peptides (Fig. 1A), but not those containing an FXXLF motif, can bind to an AR mutant in which helix 12 is removed (data not shown) suggests that the two classes of peptides interact with the receptor in a different manner. Furthermore, deletion of the AR amino terminus also compromises the binding of the RTI-specific, but not the FXXLF-containing peptides, implying that the interaction surface of the latter peptides is complex, requiring contributions from outside of the ligand binding pocket (data not shown). In accord with these findings, MD simulation experiments revealed large-scale alterations in AR structure upon binding of RTI-018 and RTI-001, which involve sites distal to the previously defined AF-2 domain (not shown). The findings of our studies underscore the importance of defining the cofactors/proteins that interact with AR in the presence of the RTI compounds, with a view to establishing a link between the structure of the AR-ligand complex, cofactor recruitment, and the regulation of gene expression. Although these studies are underway, the preliminary studies looking at recruitment of ARA54 and NCoR using a mammalian two-hybrid system indicate that the conformational changes we have observed do indeed translate into differential cofactor recruitment.

The molecular modeling approach presented here has its own limitations, such as that it cannot account for the contribution of the N-terminal portion to the stabilization of ligand- and peptide binding. Our studies indicate that this stabilization is important, as the deletion of NTD and DNA binding domain (DBD) negatively affects the binding of peptides presented in Fig. 1A, as well as ARA54 and NCoR fragments (data not shown). However, in the absence of the crystal structure of full-length AR, isolated LBD provides the best model for predicting the conformational change directed by novel ligands.

Our studies provide evidence that the biological consequence of SARM action may not require absolute changes in gene expression but occur as a result of differences in the kinetics of induction of similar genes. Indeed, the SARMs studied here either exaggerate the effects of DHT on some genes (most downregulated), or cause up-regulation of the expression of some genes with altered time-course (most early upregulated), or work as partial to full agonists (late upregulated). In agreement with these observations, the RTI SARMs have an impact on the same physiological pathways as canonical agonists but recapitulate the different facets of DHT action: strong stimulation of proliferation, similar to that caused by DHT at its most active concentration (1 nM; Fig. 7B) but weaker stimulation of lipogenesis.

It is now well accepted that ligand-induced alterations in ER structure are at the root of SERM action. However, to our knowledge, the studies presented here are the first to demonstrate that differential activation of androgen-responsive gene transcription can be accomplished using small molecules that regulate the presentation of different protein-protein interaction surfaces on AR. Thus, although the identification of the first generation of SERMs occurred in an empirical manner without an understanding of the relationship between ER structure and biological activity, the development of SARMs is likely to occur in a more rational manner. This study, therefore, establishes a firm link between AR structure and differential gene regulation; a first step in the establishment of mechanism-based screens for SARM identification.

MATERIALS AND METHODS

Affinity Selection of AR-Binding Sequences

Baculovirus-expressed full-length wt AR expressed in the presence of RTI-6413-001 was purified as described in (26). For panning, the purified receptor was diluted in 100 μl of $NaHCO_3$ (pH 8.5), applied to a single well in a 96-well Costar plate (Corning Inc. Life Sciences, Acton, MA), and incubated at 4 C overnight. The wells were blocked with 150 μl of 2% nonfat dry milk in $NaHCO_3$ for an additional 1 h at room temperature and washed five times with PBST [137 mM NaCl, 2.7 mM KCl, 4.3 mM Na_2HPO_4, 1.4 mM KH_2PO_4 (pH 7.3), 0.1% Tween 20] to remove excess protein. Then 25 μl of the phage peptide library (with >10^{10} phage particles) diluted in 125 μl of PBST with 10^{-6} M hormones and 2% milk was added to the wells, and the plate was sealed and incubated for 3 h at room temperature. Nonbinding phage were removed by washing the wells five times with PBST. The bound phage were eluted with 100 μl of 0.1 M HCl and neutralized with 100 μl of 100 mM Tris-HCl (pH 8.0). Phage eluted from the targets were amplified in *Escherichia coli* DH5αF' cells for 5 h, and the supernatant containing amplified phage was collected for use in subsequent rounds of panning. A total of four rounds of panning were performed. Enrichment of AR binding phage was confirmed by enzyme-linked immunosorbent assay. Individual phage were PCR amplified after the third panning, and shotgun cloned into pMsx vector for use in mammalian two-hybrid assay. The libraries used were constrained in the following way: X_7-L-X-X-L-L-X_7 (library 11, peptide 1132–4, Fig. 1A); X_7-L-X-X-H/I-I-X-X-X-I/L-X_7$ (library 12, peptide 1232–6 on Fig. 1A); X_6-P-X_6 (library 13, peptide 1332–4, Fig. 1A). "X" designates any amino acid, encoded by a random NNK codon. Library construction is described in (16).

Mammalian Two-Hybrid Assay

HepG2 hepatocellular carcinoma cells were seeded in 24-well plates at approximately 100,000 cells per well in MEM supplemented with 8% fetal bovine serum, nonessential amino acids and sodium pyruvate. Cells were transfected using the lipofectin reagent (Invitrogen) in OPTI-MEM with the combination of expression constructs for full-length AR (wt or

EXHIBIT H

T877A)-VP16 fusion or AR LBD (AR 624–919) (wt or T877A)-VP16 fusion, or VP16 control (1000 ng), cofactor-GAL4DBD fusion or GAL4DBD control (1000 ng), reporter construct (5×Gal4-Luc3, 900 ng) and CMV-βGal expression construct for normalization of transfection efficiency (100 ng). All plasmid quantities provided are per three wells. After 20 h, cells were washed with PBS and exposed to 10^{-7} M of hormones as indicated or ethanol vehicle in MEM supplemented with 8% charcoal-stripped fetal bovine serum with additional supplements, as above for 40 h. Interaction of AR and cofactors was assessed by measuring luciferase activity in cell lysates and normalizing it to βGal activity. Mammalian two-hybrid experiments that tested peptide binding to AR were performed in a similar manner in HepG2 cells. In this case, AR was expressed as a VP16 fusion, and the peptides as GAL4DBD fusions.

Molecular Modeling

MD simulations were performed for the AR occupied by DHT, RTI-6413-018, or RTI-6413-001. The initial geometries for simulations were provided by crystal structure 1I37 from the Protein Data Bank (27). For modeling of the T877A complex, T877 in 1I37 structure was replaced with alanine, and the resulting structure was energy minimized and equilibrated. All calculations were performed with the Amber 8.0 program (28) using the force field for protein described by Cornell *et al.* (29, 30), and General force fields (31) for the ligands. Hydrogen atoms were added to the structure using standard amino acid geometries as templates. Partial charges on the ligand molecules were fitted by using Merz-Singh-Kollman method (32, 33). The structures of AR with DHT, RTI-6413-018, and RTI-6413-001 bound were solvated by placing them into a box of TIP3P water molecules. Two thousand steps of steepest descent and 3000 steps of conjugated gradient minimization were performed. Periodic boundary and constant pressure conditions were used. Molecules were equilibrated with 2.5 nsec MD simulation, and 500 psec productive MD trajectories were analyzed using PTRAJ (34) and HARLEM programs (HARLEM, Molecular Modeling Package, http://www.kurnikov.org/harlem_main.html.)

DNA Microarray Experimental Design

LNCaP cells were grown in DMEM/8% fetal bovine serum supplemented with sodium pyruvate and nonessential amino acids in T75 flasks to approximately 70% confluence. The cells were washed with PBS three times, and the medium was replaced with phenol red-free DMEM/8% charcoal-stripped fetal bovine serum with the above supplements. After 3 d, the medium was replaced with the same medium supplemented with 10^{-8} M DHT or 10^{-7} M RTI-6413-018 or ethanol vehicle. Cells were harvested by trypsinization at 6 and 24 h and immediately frozen in liquid nitrogen. Three flasks were used per treatment, per time point, and consequently pooled to account for possible flask-to-flask variations. mRNA was isolated using the Oligotex midi kit (QIAGEN, Valencia, CA). Hybridizations were performed on the Affymetrix Hu.133AB platform. Vehicle-treated samples were exposed for the same time periods as the hormone-treated samples and used as controls. Three biological replicates were used for each treated condition.

Statistical Analysis of the Microarray Data

The analyses were performed using probe-level data. The probe intensities were extracted from CEL files by utilizing the Affymetrix Input Engine from the SAS Microarray Solution software (SAS Institute Inc.). A logarithm based 2 transformation was applied to the raw perfect-match intensities. Upon inspection of the scatter plots of pairs of chips within a replicated group, some curvature was observed (Supplemental Fig. 6). To normalize this nonlinear relationship between chips, a LOESS adjustment was applied. The normalization process was performed by running LOESS Normalization from the SAS Microarray Solution with smoothing parameter equal to 0.5. This procedure uses the mean intensities across all chips as common baseline, and fits the data from each chip to this baseline. The LOESS-normalized intensities equal the corresponding intensities of baseline plus the corresponding residual from the LOESS fit. Supplemental Fig. 6 represents the scatter plots between two replicated chips before and after normalization, respectively. After normalization, the following mixed model was applied by running Mixed Model Analysis from the SAS Microarray Solution. Refer to Ref. 35 for details on applying mixed models to probe-level data.

$$Y_{ijkl} = C_i + T_j + CT_{ij} + P_l + CP_{il} + TP_{jl} + A_k + \varepsilon_{ijkl}$$

$$A_k \sim N(0, \sigma^2_a)$$

$$\varepsilon_{ijkl} \sim N(0, \sigma^2)$$

Here, Y represents the normalized data. C, T, and P represent the treatment condition, time, and probe effects, respectively. The composite symbols represent the interactions between the corresponding effects. A and ε represent the chip random effect and stochastic error, respectively, and both are assumed to be normally distributed and independent. Indexes i, j, k, and l are associated with treatment condition, time, chip, and probe effect, respectively. Significant genes were determined by conducting Student's t tests based on the estimated parameters from this model. The specific tests consisted of differences between treatment groups across time (6 and 24 h) and between treatment groups within each time period. A Bonferroni correction was applied across all tests to control the probability of one or more false positives to be 0.05.

Real-Time PCR Quantification

Cells were treated in the same manner as used for the harvesting of mRNA for the microarray screening. In some cases, the cells were grown in 12-well plates. Cells were lysed on the plate and total RNA was isolated using the RNeasy mini kit (QIAGEN) with on-column deoxyribonuclease digest (ribonuclease-free deoxyribonuclease set, QIAGEN). First-strand cDNA was prepared using 1st strand SuperScript II synthesis kit (Invitrogen) per manufacturer's instructions using random hexamer primers. Quantitative PCR was performed using SYBR Green Supermix (Bio-Rad, Hercules, CA) in the iCycler Real-Time PCR system (Bio-Rad). The protocol used was as follows: 95 C for 5 min; 40 cycles of 95 C for 30 sec, 63 C for 30 sec, 72 C for 30 sec; 72 C for 7 min. Standard curves were prepared for each primer pair and quantification was based upon the standard curve and normalized to the housekeeping control gene (GAPDH). Each sample was analyzed in duplicate. The sequences of the primers used here are as follows:

GAPDH: forward, GGCTCTCCAGAACATCATCCCTGC; reverse, GGGTGTCGCTGTTGAAGTCAGAGG. PSA: forward, CCTCCTGAAGAATCGATTCC; reverse, GAGGTCCACACACTGAAGTT.

ABCG1: forward, CGCATCACCTCGCACATTG; reverse, TCCCGAAGAAAGACTCCCATC

HMGCS2: forward, TCGCCTGATGTTCAATGACTTC; reverse, CTTGTTGGTGTAGGTGTCTTCC. SLC16A6: forward, ACATCTTCATTCAGAGCATAGC; reverse, GTCCCATCTTACACGGTCTC. FKBP51: forward, CGGAGAACCAAACGGAAAGG; reverse, CTTCGCCCACAGTGAATGC.

EXHIBIT H

Lipogenesis Assay

LNCaP cells were seeded in 24-well plates at 160,000 cells per well in RPMI/8% charcoal-stripped fetal bovine serum supplemented with nonessential amino acids and sodium pyruvate and incubated for 3 d. Cells were induced by addition of an equal volume of the medium with 2× concentration of hormones. After 72 h, cells were fixed in 1% formaldehyde and stained with 0.3% Oil Red O in 60% isopropanol for 1 h. Cells were washed with water and absorbed Oil Red O was extracted with isopropanol. Oil Red O in extract was measured by absorbance at 490 nm. Wells with no cells in them were treated in the same way and used as a blank. An identical set of plates was seeded and treated in the same way. This set was used for monitoring of cell proliferation by direct cell counting on a Coulter counter. Accumulation of lipids was determined as Oil Red O inclusion normalized to cell number.

REFERENCES

1. Culig Z 2004 Androgen receptor cross-talk with cell signalling pathways. Growth Factors 22:179–184
2. Simoncini T, Mannella P, Fornari L, Caruso A, Varone G, Genazzani AR 2004 Genomic and non-genomic effects of estrogens on endothelial cells. Steroids 69:537–542
3. McDonnell DP 2005 The molecular pharmacology of estrogen receptor modulators: implications for the treatment of breast cancer. Clin Cancer Res 11:871s–877s
4. Norris JD, Paige LA, Christensen DJ, Chang CY, Huacani MR, Fan D, Hamilton PT, Fowlkes DM, McDonnell DP 1999 Peptide antagonists of the human estrogen receptor. Science 285:744–746
5. Shang Y, Brown M 2002 Molecular determinants for the tissue specificity of SERMs. Science 295:2465–2468
6. Jansen MS, Nagel SC, Miranda PJ, Lobenhofer EK, Afshari CA, McDonnell DP 2004 Short-chain fatty acids enhance nuclear receptor activity through mitogen-activated protein kinase activation and histone deacetylase inhibition. Proc Natl Acad Sci USA 101:7199–7204
7. Langley E, Zhou ZX, Wilson EM 1995 Evidence for an anti-parallel orientation of the ligand-activated human androgen receptor dimer. J Biol Chem 270:29983–29990
8. Kemppainen JA, Langley E, Wong CI, Bobseine K, Kelce WR, Wilson EM 1999 Distinguishing androgen receptor agonists and antagonists: distinct mechanisms of activation by medroxyprogesterone acetate and dihydrotestosterone. Mol Endocrinol 13:440–454
9. He B, Lee LW, Minges JT, Wilson EM 2002 Dependence of selective gene activation on the androgen receptor NH2- and COOH-terminal interaction. J Biol Chem 277:25631–25639
10. He B, Kemppainen JA, Wilson EM 2000 FXXLF and WXXLF sequences mediate the NH2-terminal interaction with the ligand binding domain of the androgen receptor. J Biol Chem 275:22986–22994
11. Muddana SS, Price AM, MacBride MM, Peterson BR 2004 11β-Alkyl-δ9-19-nortestosterone derivatives: high-affinity ligands and potent partial agonists of the androgen receptor. J Med Chem 47:4985–4988
12. Song LN, Coghlan M, Gelmann EP 2004 Antiandrogen effects of mifepristone on coactivator and corepressor interactions with the androgen receptor. Mol Endocrinol 18:70–85
13. Kemppainen JA, Wilson EM 1996 Agonist and antagonist activities of hydroxyflutamide and Casodex relate to androgen receptor stabilization. Urology 48:157–163
14. Chang CY, McDonnell DP 2002 Evaluation of ligand-dependent changes in AR structure using peptide probes. Mol Endocrinol 16:647–660
15. Sathya G, Chang CY, Kazmin D, Cook CE, McDonnell DP 2003 Pharmacological uncoupling of androgen receptor-mediated prostate cancer cell proliferation and prostate-specific antigen secretion. Cancer Res 63:8029–8036
16. Chang CY, Norris JD, Jansen M, Huang HJ, McDonnell DP 2003 Application of random peptide phage display to the study of nuclear hormone receptors. Methods Enzymol 364:118–142
17. Hur E, Pfaff SJ, Payne ES, Gron H, Buehrer BM, Fletterick RJ 2004 Recognition and accommodation at the androgen receptor coactivator binding interface. PLoS Biol 2:E274
18. He B, Gampe Jr RT, Kole AJ, Hnat AT, Stanley TB, An G, Stewart EL, Kalman RI, Minges JT, Wilson EM 2004 Structural basis for androgen receptor interdomain and coactivator interactions suggests a transition in nuclear receptor activation function dominance. Mol Cell 16:425–438
19. Swinnen JV, Van Veldhoven PP, Esquenet M, Heyns W, Verhoeven G 1996 Androgens markedly stimulate the accumulation of neutral lipids in the human prostatic adenocarcinoma cell line LNCaP. Endocrinology 137:4468–4474
20. Love RR, Mazess RB, Barden HS, Epstein S, Newcomb PA, Jordan VC, Carbone PP, DeMets DL 1992 Effects of tamoxifen on bone mineral density in postmenopausal women with breast cancer. N Engl J Med 326:852–856
21. Delmas PD, Bjarnason NH, Mitlak BH, Ravoux AC, Shah AS, Huster WJ, Draper M, Christiansen C 1997 Effects of raloxifene on bone mineral density, serum cholesterol concentrations, and uterine endometrium in postmenopausal women. N Engl J Med 337:1641–1647
22. Ettinger B, Black DM, Mitlak BH, Knickerbocker RK, Nickelsen T, Genant HK, Christiansen C, Delmas PD, Zanchetta JR, Stakkestad J, Gluer CC, Krueger K, Cohen FJ, Eckert S, Ensrud KE, Avioli LV, Lips P, Cummings SR 1999 Reduction of vertebral fracture risk in postmenopausal women with osteoporosis treated with raloxifene: results from a 3-year randomized clinical trial. Multiple Outcomes of Raloxifene Evaluation (MORE) Investigators. JAMA 282:637–645
23. McDonnell DP, Connor CE, Wijayaratne A, Chang CY, Norris JD 2002 Definition of the molecular and cellular mechanisms underlying the tissue-selective agonist/antagonist activities of selective estrogen receptor modulators. Recent Prog Horm Res 57:295–316
24. McDonnell DP 2004 The molecular determinants of estrogen receptor pharmacology. Maturitas 48:7–12
25. Kauppi B, Jakob C, Farnegardh M, Yang J, Ahola H, Alarcon M, Calles K, Engstrom O, Harlan J, Muchmore S, Ramqvist AK, Thorell S, Ohman L, Greer J, Gustafsson JA, Carlstedt-Duke J, Carlquist M 2003 The three-dimensional structures of antagonistic and agonistic forms of

EXHIBIT H

the glucocorticoid receptor ligand-binding domain: RU-486 induces a transconformation that leads to active antagonism. J Biol Chem 278:22748–22754

26. Juzumiene D, Chang C-y, Fan D, Hartney T, Norris JD, McDonnell DP 21 October 2005 Single-step purification of full-length human androgen receptor. Nucl Recept Signal 10.1621/nrs.03001

27. Sack JS, Kish KF, Wang C, Attar RM, Kiefer SE, An Y, Wu GY, Scheffler JE, Salvati ME, Krystek Jr SR, Weinmann R, Einspahr HM 2001 Crystallographic structures of the ligand-binding domains of the androgen receptor and its T877A mutant complexed with the natural agonist dihydrotestosterone. Proc Natl Acad Sci USA 98:4904–4909

28. Case DA, Cheatham TE, Darden T, Gohlke H, Luo R, Merz Jr KM, Onufriev A, Simmerling C, Wang B, Woods RJ 2005 The Amber biomolecular simulation programs. J Comput Chem 26:1668–1688

29. Cornell WD, Cieplak P, Bayly CI, Gould IR, Merz KM, Ferguson DM, Spellmeyer DC, Fox T, Caldwell JW, Kollman PA 1995 A 2nd generation force-field for the simulation of proteins, nucleic-acids, and organic-molecules. J Am Chem Soc 117:5179–5197

30. Kollman P, Dixon R, Cornell W, Fox T, Chipot C, Pohorille A 1997 The development/application of a "minimalist" organic/biochemical molecular mechanic force field using a combination of ab initio calculations and experimental data. In: Wilkinson A, Weiner P, van Gunstren WF, eds. Computer simulation of biochemical systems. Vol 3. New York: Elsevier; 83–96

31. Wang JM, Wolf RM, Caldwell JW, Kollman PA, Case DA 2004 Development and testing of a general amber force field. J Comput Chem 25:1157–1174

32. Singh UC, Kollman PA 1984 An approach to computing electrostatic charges for molecules. J Comput Chem 5:129–145

33. Besler BH, Merz KM, Kollman PA 1990 Atomic charges derived from semiempirical methods. J Comput Chem 11:431–439

34. Pearlman DA, Case DA, Caldwell JW, Ross WS, Cheatham TE, Debot S, Ferguson D, Seibel G, Kollman P 1995 Amber, a package of computer-programs for applying molecular mechanics, normal-mode analysis, molecular-dynamics and free-energy calculations to simulate the structural and energetic properties of molecules. Comput Physics Commun 91:1–41

35. Chu TM, Weir B, Wolfinger R 2002 A systematic statistical linear modeling approach to oligonucleotide array experiments. Math Biosci 176:35–51

36. Chang CY, Walther PJ, McDonnell DP 2001 Glucocorticoids manifest androgenic activity in a cell line derived from a metastatic prostate cancer. Cancer Res 61: 8712–8717